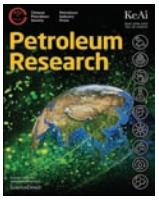
Petroleum Research 11 (2026) 217–236

Contents lists available at ScienceDirect

Petroleum Research

journal homepage: http://www.keaipublishing.com/en/journals/petroleum-research/



Full Length Article

Estimation of fluid saturation and pressure distribution throughout a reservoir using machine learning techniques



Arifur Rahman [a], George Daoud [b,c], Ezeddin Shirif [a,*], Mohamed El-Darieby [b], Mohamed El-Hendawi [c,d]

[a] Petroleum Systems Engineering, Faculty of Engineering and Applied Science, University of Regina, Regina, S4S 0A2, SK, Canada
[b] Faculty of Engineering and Applied Science, Ontario Tech University, Oshawa, L1G 0C5, ON, Canada
[c] Electrical Engineering Department, Assiut University, Assiut, 71515, Egypt
[d] Electronic Systems Engineering, University of Regina, Regina, S4S 0A2, SK, Canada

ARTICLE INFO

Article history:
Received 25 January 2024
Received in revised form
18 August 2025
Accepted 27 August 2025
Available online 2 September 2025

Keywords:
Fluid saturation
Pressure distribution
Feedforward neural network
Convolutional neural network
Deep neural network

ABSTRACT

Water saturation is one of the most critical yet often underappreciated petrophysical parameters in reservoir characterization. A wide range of petrophysical and reservoir engineering computations that lead to crucial field development decisions, including reserve estimation, waterflooding efficiency calculation, and capillary pressure deduction, rely on its accurate determination. This study demonstrates how machine learning techniques can forecast reservoirs' fluid saturation and pressure distribution. This study describes a deep learning–based proxy modeling technique for accurately predicting reservoir pressure distribution and fluid (oil, water, and gas) saturation during water flooding in single-layer heterogeneous reservoirs. This study used recurrent neural networks (RNNs) and convolutional neural networks (CNNs) to build a proxy model. This work indicates that compared to simulation outcomes, computer-based machine learning algorithms can accurately predict fluid (oil, water, and gas) saturation and pressure distribution. The stated accuracy was evaluated numerically and graphically, and error analysis between various machine learning approaches and simulated results was utilized.

© 2025 Chinese Petroleum Society. Publishing services by Elsevier B.V. on behalf of KeAi Communications Co. Ltd. This is an open access article under the CC BY-NC-ND license (http://creativecommons.org/licenses/by-nc-nd/4.0/).

1. Introduction

Throughout the oilfield development process, reservoirs frequently have a considerable volume of residual oil due to reservoir heterogeneity and diverse production modes. As a result, predicting the residual oil or water saturation distribution is critical for future oilfield development (Glushkov et al., 2021). The ability to accurately estimate reservoir propertiesin a reservoir makes it easier to tap the residual oil. There are two main conventional approaches to analyzing and estimating water saturation. The first approach is to use a petrophysical model to measure the reservoir's water saturation. Archie (1947) calculated water saturation (Sw) in the reservoir using formation resistivity and porosity. Others used capillary pressure data and computed water saturation using saturation–height functions, such as the Heseldin system (Heseldin, 1974) or the Leverett J function (Leverett, 1941).

These methods take a long time to execute, and their sampling range does not accurately match the reservoir. The second approach is numerical simulation, which is commonly used in the petroleum industry. Several simulation techniques have emerged for various development scenarios and reservoir sizes (Chen et al., 2006; Ertekin et al., 2001; Karimi-Fard et al., 2004; Riviere, 2007). At this point, reservoir modeling plays a significant role in formulating reservoir development plans and optimizing oil recovery (Edwards et al., 2011). In this context, many researchers have used numerical modeling to study water saturation distribution for a variety of problems, including water imbibition (Almulhim et al., 2014; Tuero et al., 2017; Zhang et al., 2018), the performance of enhanced oil recovery (EOR) approaches (Al-Zawawi et al., 2011; Yuan et al., 2010), unconventional reservoir exploitation (Liu et al., 2017; Liu and Wu, 2015), and so on. AI applications are becoming more prevalent in numerous petroleum engineering disciplines, such as reservoir characterization (Mohaghegh et al., 2000), PVT (Pressure Volume Temperature)

* Corresponding author.
E-mail address: ezeddin.shirif@uregina.ca (E. Shirif).
Peer review under the responsibility of Editorial Office of Petroleum Research.

https://doi.org/10.1016/j.ptlrs.2025.08.007
2096-2495/© 2025 Chinese Petroleum Society. Publishing services by Elsevier B.V. on behalf of KeAi Communications Co. Ltd. This is an open access article under the CC BY-NC-ND license (http://creativecommons.org/licenses/by-nc-nd/4.0/).

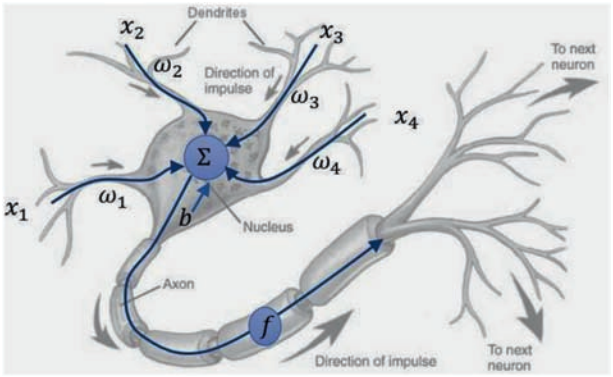


Fig. 1. Artificial neuron vs. biological neuron (Patoary et al., 2015; Zhang, 2019).

data prediction (Gharbi and Elsharkawy, 1997), well log interpretation (Baldwin et al., 1989; Lim and Kim, 2004), well test data analysis (Sultan and Al-Kaabi, 2002; Rahman, 2012; Rahman et al., 2017a, 2017b), seismic characteristics (Roth and Tarantola, 1992), fault detection (Omurlu et al., 2012; Sadiq and Nashawi, 2007), and formation damage prognosis (Nikravesh et al., 1996; Samuel, 2000; Zhou et al., 1994).

Owing to the boom of big data and data analytic methods to simplify certain operations, minimize cost, and increase efficiency, machine learning (ML) has become a fast-growing topic in every industry, including the oil and gas industry. Machine learning is a subdiscipline of artificial intelligence that refers to a class of mathematical algorithms that can "learn" from existing data without specific programming. These algorithms can be used to create models that can forecast the result of a series of circumstances. Completion, formation, and fluid parameters are the conditions in this case. Samuel (2000) described machine learning as the area of research that enables computers to learn without being directly taught or programmed. Nagi et al. (2009) concluded that ML algorithms can be used to evaluate fluid properties instead of collecting extensive fluid data in each reservoir to decide specific key parameters essential for in-field oil or gas production. Field development plans and resource assessment are heavily influenced by initial hydrocarbon saturation. However, reservoir propertiesis calculated using indirect measurements from spatially dispersed wells and saturation height modeling with unknown parameters. This paper uses various neural network architectures to develop predictive models that can accurately estimate fluid saturation and pressure distribution throughout a reservoir.

2. Background

In 1952, Nobel Prize winners Sir Alan Lloyd Hodgkin and Sir Andrew Fielding Huxley successfully decoded the functionality and mechanism of the neurons of a giant squid. They built the first mathematical and electric model to simulate a biological neuron (Tian and Zhou, 2021). Fig. 1 shows a biological neuron that consists of four major parts: dendrites, soma (cell body), axons, and synapses. The nerve signal was found to be a sort of electrical signal generated due to the different concentrations of chemical electrolytes. Each neuron receives these signals from other neurons within its dendrites as a current ranging from −5 to 12 nA. The current flow accumulates the charge within the soma until a particular membrane potential is reached. Then, a charge spike moves across the cell's axon, activating the synapses to release electrolytes to other neurons. Learning is achieved by adjusting the number of chemicals released from each neuron and transmitted to others. Thus, the learned information is embedded in the rate of the activated signals within the cell.

Researchers took advantage of this discovered mechanism of the nervous system and tried to mimic and combine it with the traditional nonlinear regression models to form an artificial neural network (ANN) (Zhang, 2019). As shown in Fig. 1, the inputs to artificial neurons are similar to the signals received by the dendrites. At the same time, the summation (Σ) acts like the accumulation of charge within the cell. The nonlinear activation function (f) simulates the nonlinearity in the spike's characteristics. The weights (ω_i) indicate the input signals' strength (x_i). As in the biological nervous system, weights are the key to tuning the neurons to learn features and estimate a specific output. A neural network (NN) usually consists of multiple neurons connected in a feedforward layered architecture. Each neuron in this architecture has its own set of weights.

To adjust these weights, a supervised learning approach is applied in which pairs of input and output are provided to the neural network model, and a learning algorithm is used to update the values of the weights in a manner that reduces the error between the neural network estimated output and the expected output. This is done by decreasing the weights proportional to the error derivative using gradient descent (Du et al., 2019). However, training a model in this way may result in overfitting problems, in which the model learns the output and any noise in that output. To overcome this, the dataset must be divided into training and testing datasets. The learning algorithm uses only the training part to tune the model parameters, while the test dataset evaluates the model accuracy. As the learning error is likely to decrease during the learning process, the best parameters for the model result from a minimum testing error. Thus, it is guaranteed that the model learns the actual characteristics and will work fine for any data, not only those used in the training.

The previously described neural network is called a shallow neural network due to the small number of layers and neurons in each layer. Much success has been achieved with shallow neural networks in many fields with acceptable accuracy, but their performance was poor in complex problems such as computer vision. This situation changed in 2000 when new types of NN architecture called deep neural networks (DNNs) and recurrent neural networks (RNNs) were introduced (Aizenberg et al., 2000). Inspired by the human brain, researchers have used complex neural network models with many neurons per layer and many layers in deep learning models. Massive datasets are used to train these models after overcoming some technical problems in DNN, like the problem of vanishing or exploding gradients. The performance of DNNs in solving complex problems increases and overwhelms other approaches. During the development of DNNs, a new type of NN architecture called convolutional neural networks (CNNs) evolved. CNNs (Smith and Topin, 2016) consist of convolutional

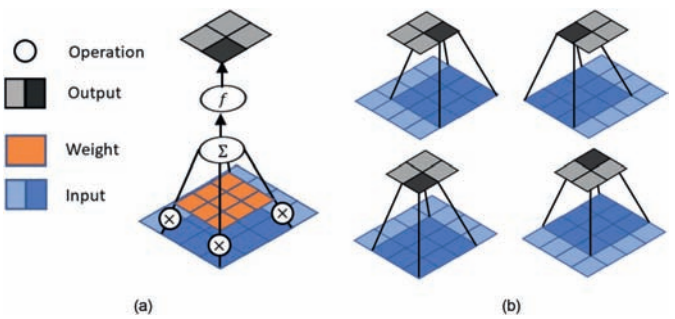


Fig. 2. Convolutional neural network.

Table 1
The dataset features collected from the CMG simulator.

Static Data	Grid block locations (*x*,*y*,*z*)
	Reservoir layers
	Porosity
	Permeability
Calculated Data	Distance of each grid block from the production well
Dynamic Data	Pressure for each grid block
	Gas, water, and oil saturations for each block

layers and are usually applied to images or any inputs represented in a spatial matrix format, as shown in Fig. 2a. In CNNs, the same model is used to rectangle part of the image to produce an output, and this model is then shifted to scan the whole image, as illustrated in Fig. 2b. Many terminologies and parameters are associated with CNN, such as padding, which is expanding a border with zero values with the goal of producing an output image with the same exact dimensions as the input image. CNNs were first used to solve handwritten digit-recognition problems (Ciregan et al., 2012) and were then used to address many other issues, such as flow in physical processes (Tu et al., 2019; Rahman et al., 2020; Rahman et al., 2017a, 2017b).

Applying deep learning approaches to forecast dynamic reservoir behaviors, particularly in EOR processes, has advanced significantly in recent years. Heterogeneous permeability distributions and facie changes are two examples of complicated spatial properties that can be captured by CNNs. Moreover, predicting the temporal dynamics of production factors such as pressure and saturation using RNNs has shown promise, especially long short-term memory (LSTM) architectures. In order to create data-driven models that can predict production dynamics without the use of conventional recursive numerical solvers, a number of studies have also investigated combinations of CNNs and RNNs.

However, few of the hybrid CNN–RNN approaches that are currently in use have specifically addressed the spatiotemporal prediction of local pressure and saturation distributions within heterogeneous water-flooded reservoirs. Instead, the majority of these approaches concentrate on the time-series prediction of global production indicators, such as cumulative oil production or water cut. Furthermore, even if these models are good at capturing the dynamics of production, they frequently consider temporal and geographical variables separately, or they need a lot of computing power and training data to generalize across different geological contexts.

We suggest a novel two-stage hybrid deep learning approach to fill these gaps. In order to effectively learn the spatial patterns of reservoir heterogeneity and their impact on flow behavior, we first build a proxy model utilizing CNN-based architectures. The model is able to capture localized interactions between fluid characteristics and rock because of this spatial encoding. Next, we include this spatially informed representation in an RNN module that simulates the time-varying fluid saturation and pressure distributions. Our method enhances the accuracy and effectiveness of predictions in extremely diverse settings by concurrently learning spatial and temporal information in a single framework.

This work builds upon and enhances earlier works in a number of significant ways. First, rather than providing overall performance measurements, it offers fine-scale spatial-temporal predictions of pressure and saturation fields. Second, it offers potential benefits in real-time reservoir management and scenario screening by introducing an effective and generalizable proxy modeling strategy that lessens reliance on extensive simulation runs and allows prediction across various reservoir settings without retraining from scratch.

Table 2
Input and output parameters of the NN model for the first scenario.

Input	Output
Distance from the well	Block pressure (t)
Block pressure (*t*-1)	Block fluid saturations (*t*)
Block fluid saturation (*t*-1)	
Well pressure (*t*-1)	
Well fluid saturations (*t*-1)	
Well pressure (*t*)	
Well fluid saturations (*t*)	

Table 3
Architecture for pressure and saturation networks for the first scenario.

	Pressure model	Fluid saturation model
1st hidden layer	16 neurons with ReLU activation function	16 neurons with ReLU activation function
2nd hidden layer	16 neurons with Tanh activation function	16 neurons with Tanh activation function
3rd hidden layer	16 neurons with ReLU activation function	16 neurons with ReLU activation function
4th hidden layer	16 neurons with Tanh activation function	16 neurons with Tanh activation function
5th hidden layer	16 neurons with ReLU activation function	16 neurons with ReLU activation function
Output layer	One neuron with Sigmoid activation function	3 neurons with SoftMax activation function

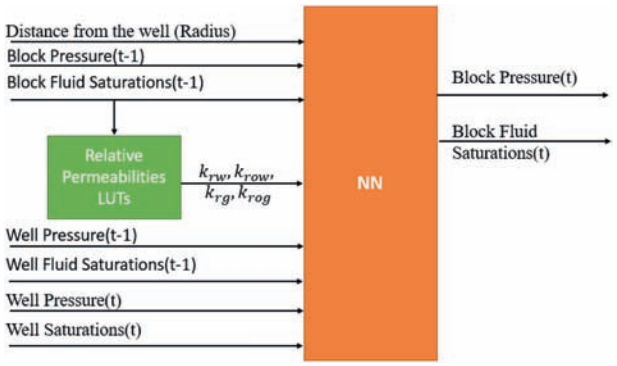


Fig. 3. Integration of relative permeability LUTs with the NN model.

Table 4
Input and output parameters of the NN model.

Input	Output
Distance from the well	Block pressure (t)
Block pressure (*t*-1)	Block fluid saturations (*t*)
Block fluid saturation (*t*-1)	
Well pressure (*t*-1)	
Well fluid saturations (*t*-1)	
Well pressure (*t*)	
Well fluid saturations (*t*)	
Block relative permeability (*t*-1) {*krg*,*krog*,*krw*,*krow*}	

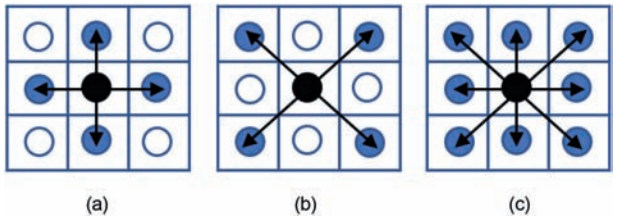


Fig. 4. Three neighbor modes in a single-layer reservoir: (a) 4-adjacent neighbors, (b) 4-diagonal neighbors, and (c) 8-surrounding neighbors.

Table 5
Dataset inputs and outputs for the third scenario.

Input	Output
Block location, porosity, and permeabilities	Block pressure (t)
Block pressure (*t*-1)	Block fluid saturations
Block fluid saturation (*t*-1)	(*t*)
Well pressure (*t*-1)	
Well fluid saturations (*t*-1)	
Well pressure (*t*)	
Well fluid saturations (*t*)	
Block relative permeability (*t*-1)	
Neighbor blocks' location, porosity, and permeabilities	
Neighbor blocks' relative permeability (*t*-1)	
Neighbor blocks' pressure (*t*-1)	
Neighbor blocks' fluid saturations (*t*-1)	

Table 6
Architecture for pressure and saturation networks.

	Pressure model	Fluid Saturation model
1st hidden layer	83 neurons with ReLU activation function	83 neurons with ReLU activation function
2nd hidden layer	83 neurons with Tanh activation function	83 neurons with Tanh activation function
3rd hidden layer	83 neurons with ReLU activation function	83 neurons with ReLU activation function
4th hidden layer	83 neurons with Tanh activation function	83 neurons with Tanh activation function
5th hidden layer	83 neurons with ReLU activation function	83 neurons with ReLU activation function
Output layer	1 neuron with Sigmoid activation function	3 neurons with SoftMax activation function

3. Methodology

This paper estimates pressure and fluid saturation distribution changes within the reservoir during production. Because the pressure difference is the main reason for all the flows within the reservoir, the estimation of fluid saturation behavior is done in parallel with that of the pressure. The data necessary to train and test the model are generated from numerical simulator software (CMG). The proposed workflow to design the neural network model consists of five steps:

(1) Run CMG for a long time (10 years) over the given reservoir and generate a tabulated format, as shown in Table 1.
(2) Preprocess the data to generate a tabular dataset as input and output pairs. Each record contains the temporal and spatial information that is ready to be fed to the NN model for training and testing purposes.
(3) Normalize the input and output data to have the same mean and standard deviation. Divide the dataset into 50 % training and 50 % testing sets.
(4) Design an NN model by adjusting its layers, the number of neurons per layer, and the activation function for each layer. Use only the training set to tune the model parameters while using the testing set to evaluate the trained model.
(5) Repeat the last two steps until a model with acceptable performance is reached.

For this study, we considered five scenarios: two concerning radial models and three concerning cartesian reservoir models. Both homogeneous and heterogeneous reservoirs are handled in these scenarios. Additionally, the effect of relative permeability is considered in four scenarios. These scenarios are described in the following subsections.

We chose 83 neurons to handle the heterogeneous reservoir case after conducting a number of empirical tuning tests to strike a balance between prediction performance and model complexity.

Table 7
Block parameter range.

Parameter	Minimum value	Maximum value
Porosity	0.18	0.35
permeability *I*	750	1000
permeability *J*	750	1000
permeability *k*	75	100

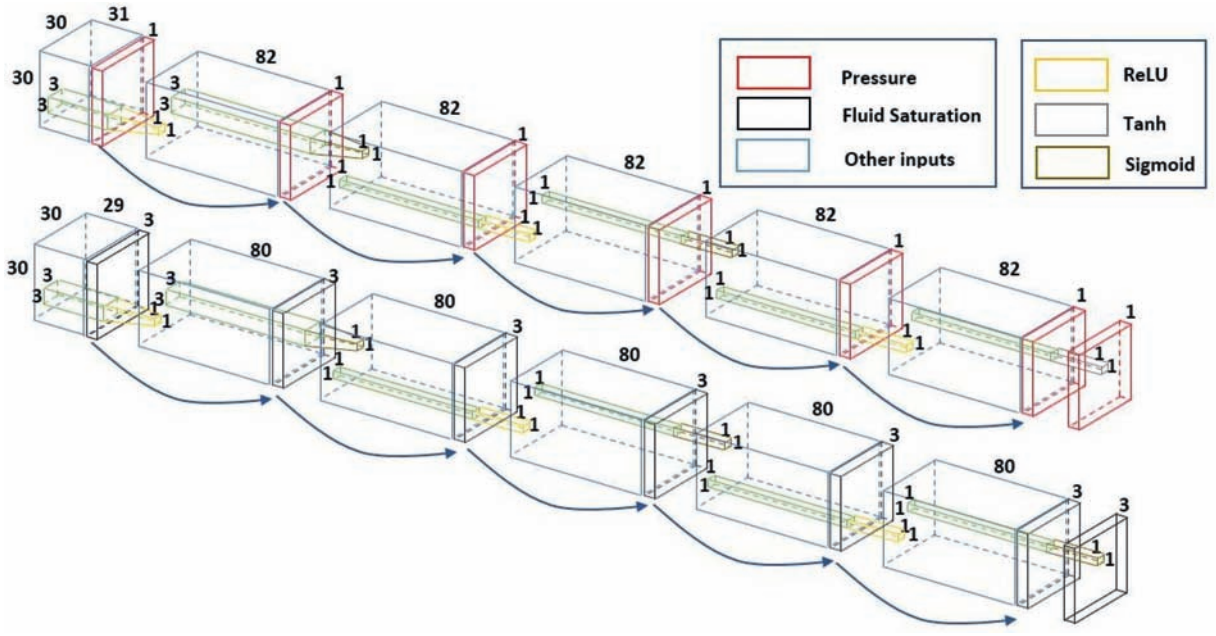


Fig. 5. CNN architecture.

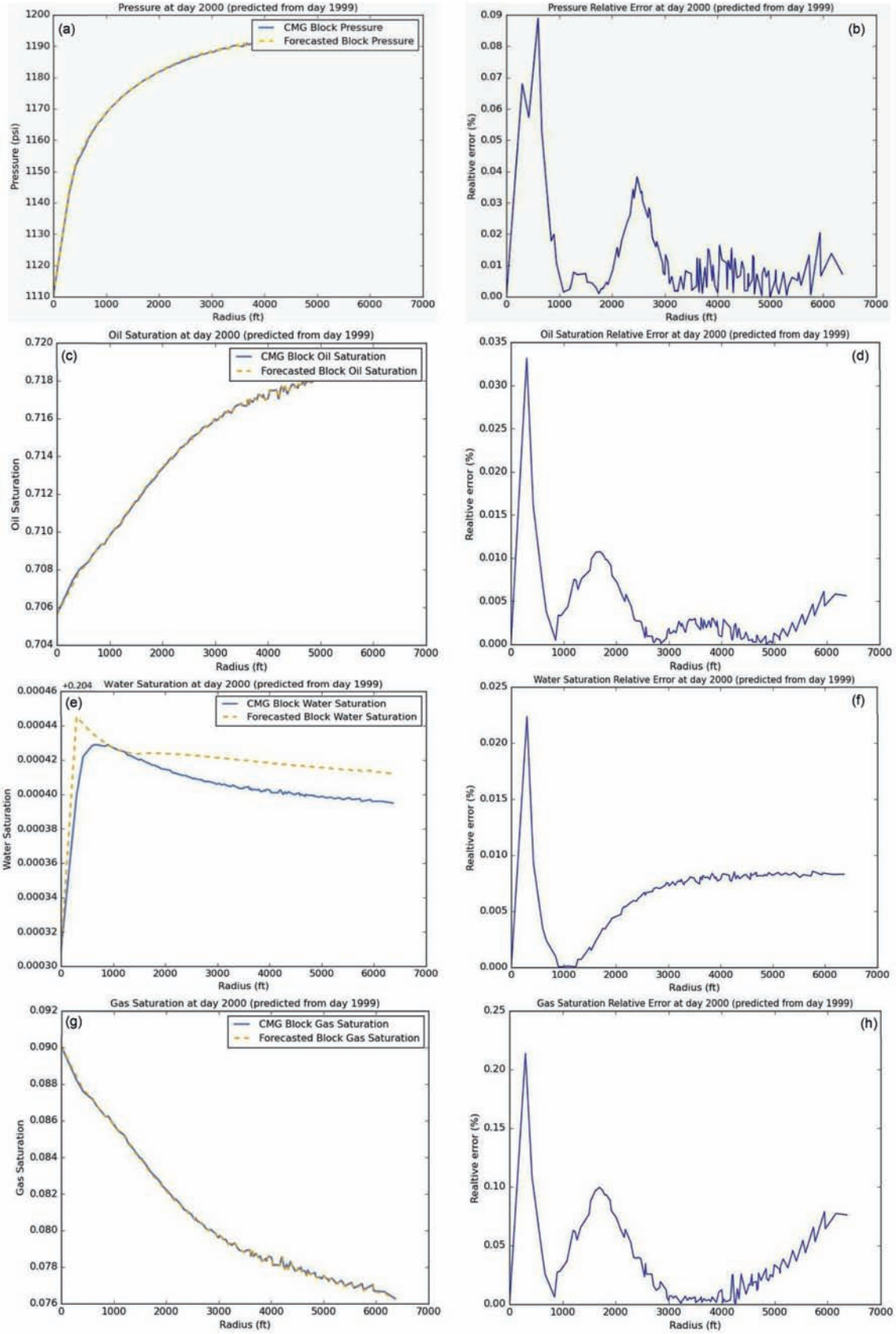


Fig. 6. One-day prediction rock and fluid properties for the first scenario.

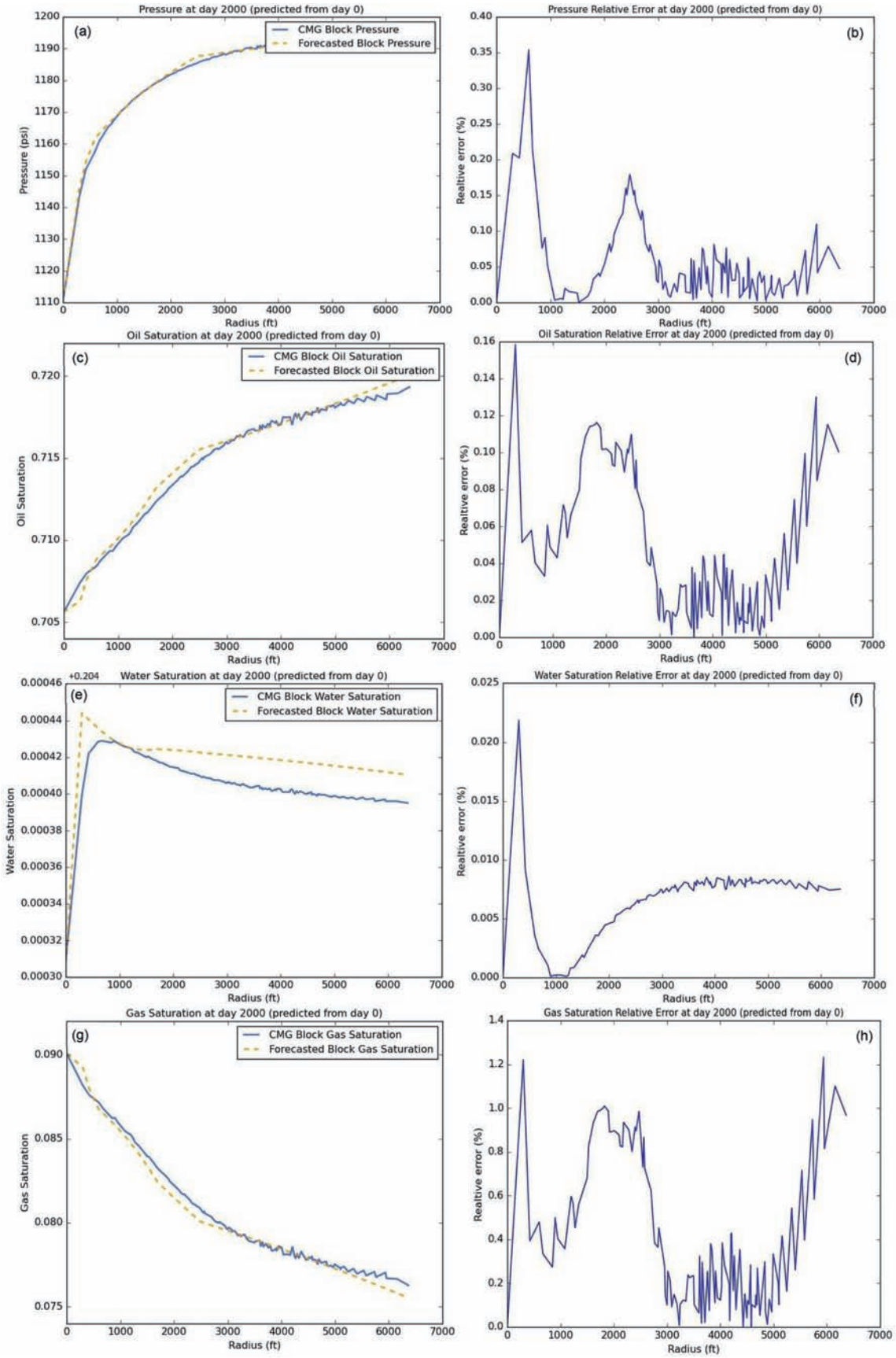


Fig. 7. 2000-day prediction rock and fluid properties for the first scenario.

Table 8
Mean absolute percentage error value for each output prediction.

	Training data (50 %)	Testing data (50 %)
Pressure	0.019215 %	0.019317 %
Oil saturation	0.004579 %	0.004571 %
Water saturation	0.008108 %	0.008110 %
Gas saturation	0.139461 %	0.139323 %

Given the geographic resolution and complexity present in our diverse datasets, this number was determined to provide the optimum trade-off between underfitting and overfitting. The network must extract and express more detailed spatial correlations in heterogeneous reservoirs due to the more complex spatial variability in parameters such as permeability and porosity; this is why the design is a little larger and deeper than in the homogeneous case. Concerning the application of Tanh and ReLU alternating activation functions: We made this deliberate decision because we wanted to preserve gradient flow stability throughout training while still capturing nonlinear interactions. Although ReLU functions are good at managing sparsity and accelerating convergence, deep layers may experience the “dying neuron” issue. Artificial neurons that stop responding or updating because their output becomes stuck at zero are frequently are referred to as “dying neurons” in artificial neural networks (common in ReLU activation functions), network learning is so constrained. In contrast, Tanh provides smoother transitions and performs better when mapping input features into a normalized range, especially when dealing with spatial data that fluctuates, as is the situation in heterogeneous reservoirs. We sought to capitalize on the advantages of both by switching between these functions, allowing the network to acquire intricate features while avoiding training problems such as dead activations or disappearing gradients.

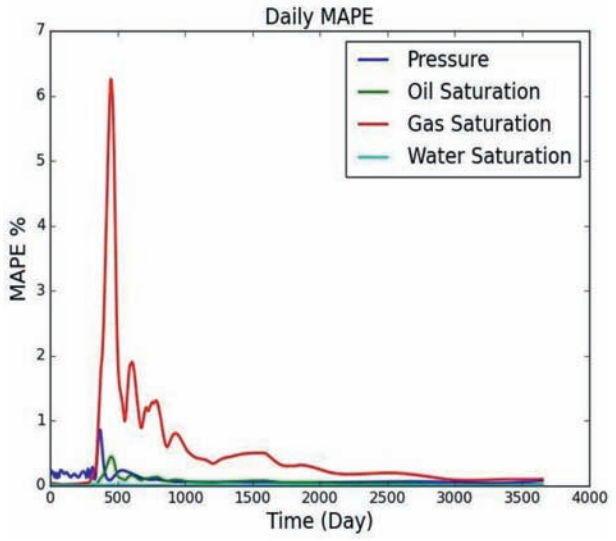


Fig. 8. The accumulated MAPE of the fluid flow for first scenerio.

Table 9
Mean absolute percentage error value for each output prediction.

	Training data (50 %)	Testing data (50 %)
Pressure	0.050315 %	0.050296 %
Oil saturation	0.017106 %	0.017081 %
Water saturation	0.019896 %	0.019956 %
Gas saturation	0.463798 %	0.465348 %

3.1. Fluid flow for a homogeneous radial model ignoring relative permeability

In this scenario, a neural network model that predicts the daily variation of the pressure and fluid saturations in a homogeneous reservoir is proposed. We assumed that the reservoir consists of one layer with 120 ring-shaped grid sectors. Due to the homogeneity of the reservoir, the flow is uniform and symmetric in a radial pattern. This means that different sectors will have the same pressure and fluid flow if they have the same distance from the well. When analyzing fluid flow toward a well in reservoir engineering and well hydraulics, the distance from the wellbore frequently determines the pressure and flow characteristics at any given point in the reservoir, presuming that the reservoir's characteristics are homogeneous and isotropic (uniform in all directions). This model can also estimate the pressure and fluid distribution throughout cartesian reservoirs by combining cartesian grid blocks with the same distance from the production well into the same radial sector. The input and output variables of the model are shown in Table 2.

Due to the radial approximation of the reservoir, a deep neural network with only feedforward layers is used. As summarized in Table 3, the proposed model reflects spatial and temporal information. The spatial information is embedded in the distance from the well. Due to the homogeneity and symmetry of the reservoir model, this simple spatial information is sufficient to estimate the output. At the same time, the temporal information is provided as the values of the pressure and fluid saturations on the previous day ($t-1$). A vital constraint when designing this architecture is that the sum of all fluid saturation should equal 1. This is achieved by using a SoftMax activation function for the output layer of the saturation model. The SoftMax function treats its outputs as probabilities to ensure that their sum is 1, which is suitable for our model. Normalization is another crucial step in which all the input and output variables are normalized to have approximately the same average and variance. This process is necessary to accelerate the model training process. However, to maintain the fluid saturation constraint, fluid saturation values in both inputs and output should not pass through the normalization process and should be considered naturally normalized data.

3.2. Fluid flow for a homogeneous radial model by considering relative permeability

One of the shortages in the previous model is that the relative permeability was ignored. The neural network model was left to predict and calculate these values in some intermediate layer when needed during the training phase. However, this assumption is not useful in the case of a heterogeneous reservoir or when the model is applied to another reservoir with different relative permeability tables. Therefore, relative permeability is included as an additional input parameter, as shown in Table 2. Relative permeability is calculated using lookup tables (LUTs). Interpolation is used to estimate the intermediate values within the given input range of the LUTs, while a hard limit is used for those values outside the input range of the LUTs. Fig. 3 illustrates how the LUTs are integrated with the neural network model input. The model shown in Table 3 is used for this scenario. In the data normalization step, the maximum and minimum values of the relative permeability are taken from the LUTs, not from the trained data.

3.3. Fluid flow prediction for a cartesian single-layer homogeneous reservoir using a DNN

A Cartesian homogeneous reservoir consisting of one layer with 30 grid blocks in both x and y directions is utilized in this scenario.

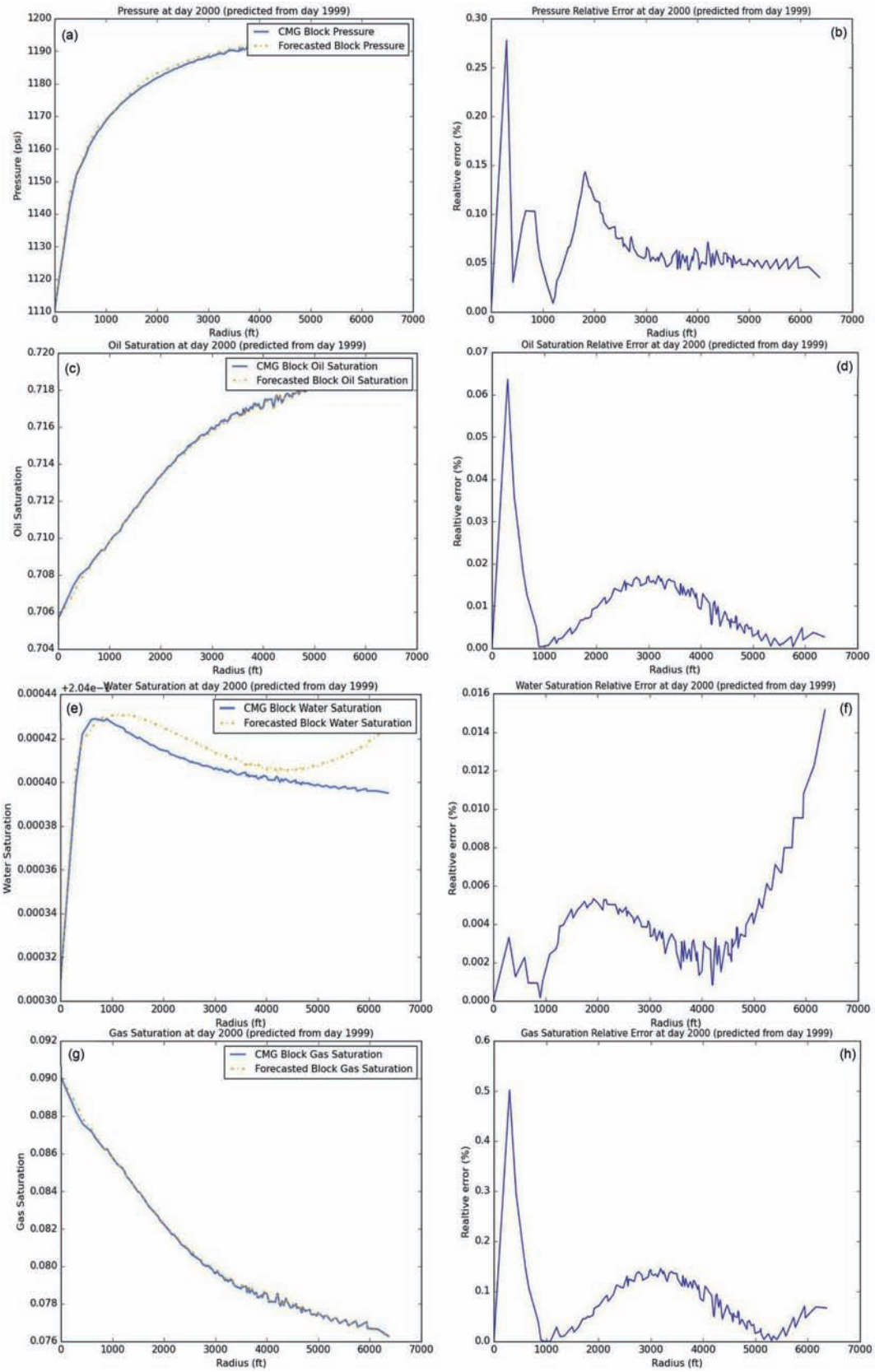


Fig. 9. One-day prediction rock and fluid properties for the second scenario.

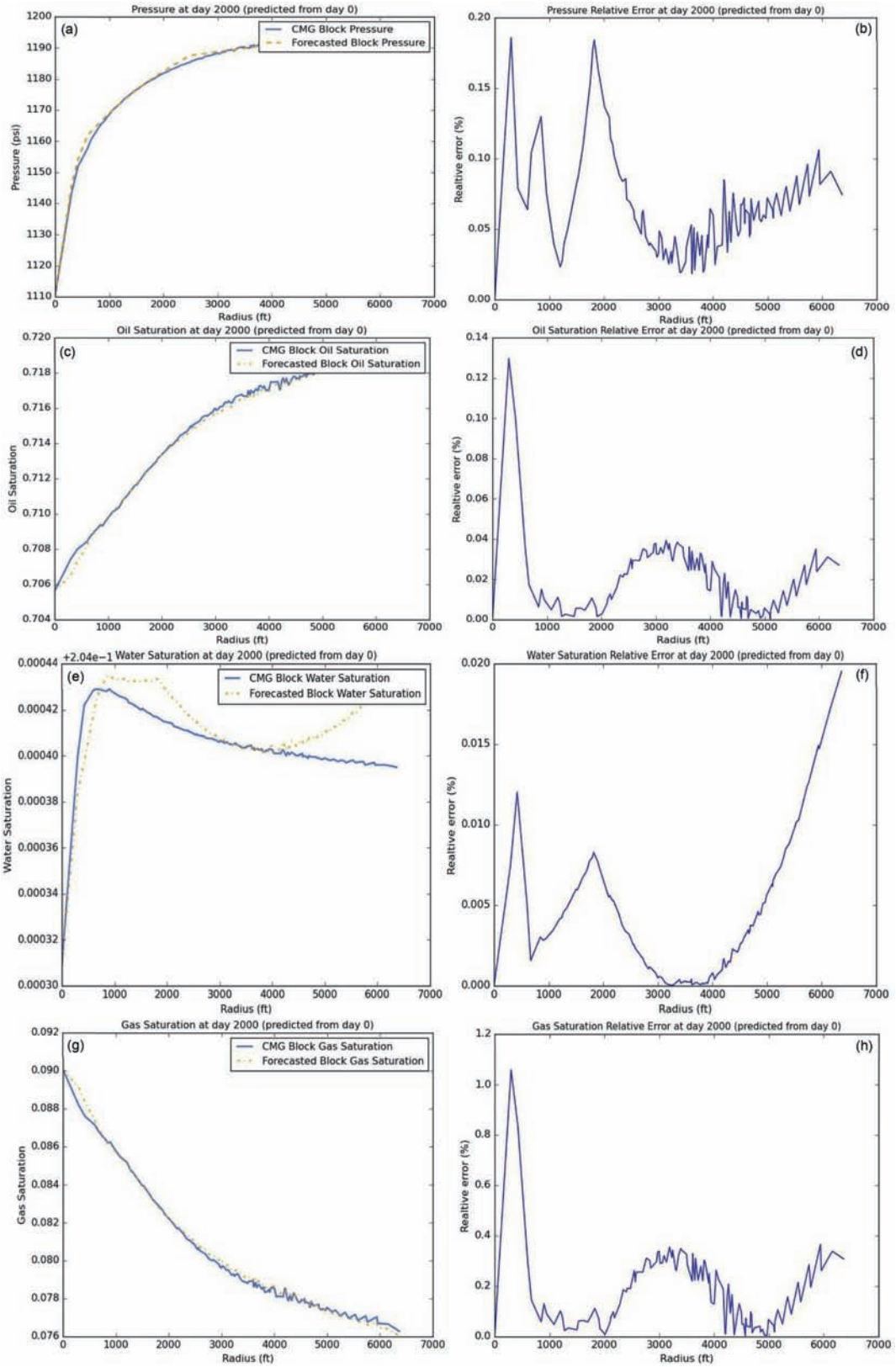


Fig. 10. 2000-day prediction rock and fluid properties for the second scenario.

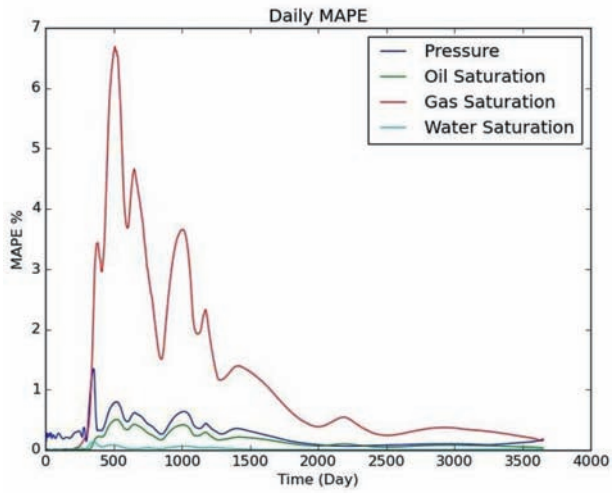


Fig. 11. The accumulated MAPE of the fluid flow for second scenerio.

Each block has a cuboid shape with the same dimensions. Relative permeabilities are also included in the model to provide more flexibility in adjusting its values through the LUTs. The input and output of this model are similar to those listed in Table 4. As shown in the table, temporal information is included as the previous day's pressure and fluid saturation values. The only difference is that the spatial information is provided by the distance between the well and the center of each block described by the Euclidian distance as well as the x and y components of that distance. This allows the model to consider different permeabilities in each direction. The architecture of the proposed model is also the architecture provided in Table 3. The only change is the number of inputs to the first layer. This is logical because the radial model used in the first two scenarios can be considered an approximation of a Cartesian model of a homogeneous reservoir.

3.4. Fluid flow prediction for a cartesian single-layer heterogeneous reservoir using a DNN

In the fourth scenario, a heterogeneous reservoir is used to create the dataset. The heterogeneity of this reservoir is guaranteed by randomly sampling the porosity and permeability of each block in the three basic directions from uniform distributions. Uniform distributions are chosen to ensure that the sampled values are distributed over the whole possible range. This contributes to training a general model that can handle any possible values of porosity and permeability. Additionally, the uniform distributions have a hard limit to the values to keep them within the acceptable range.

Due to the heterogeneity, the blocks' pressure and fluid distribution cannot be estimated only using the information of the well block but also with the neighbor blocks. For a single-layer reservoir, only neighbors in two dimensions are required. Thus, there are three choices for neighbors, as shown in Fig. 4. Two consider only the four nearest neighbors in adjacent or diagonal directions. The third handles all eight possible neighbors. The pressure, fluid saturation, and relative permeabilities of the 4-adjacent neighbors (Fig. 4a) on the previous day are additional inputs to the model. Therefore, the model can learn complicated spatial-temporal patterns. Moreover, the porosity and permeability of the five blocks (neighbors and the current blocks) are fed as inputs to the model because of the heterogeneous nature of the reservoir. Table 5 lists both the input and output variables for this model.

Table 10
Mean absolute percentage error value for each output prediction.

	Training data (50 %)	Testing data (50 %)
Pressure	0.013085 %	0.013049 %
Oil saturation	0.007446 %	0.007442 %
Water saturation	0.008236 %	0.008229 %
Gas saturation	0.187085 %	0.186719 %

A DNN model with multiple layers and many nodes per layer, shown in Table 6, is proposed for such a complicated issue to learn such a large amount of information. The activation functions in each layer are chosen carefully to eliminate gradient decaying or saturation problems. The ReLU activation function is used in some layers as it does not suffer from these problems. Furthermore, the Tanh activation functions are used to produce normalized values with a higher probability of having a zero mean and standard deviation. This improves the speed of learning.

3.5. Fluid flow prediction for a cartesian single layer heterogeneous reservoir using a CNN

Using the previously proposed model for solving the heterogeneous reservoir can capture the reservoir's performance. Preparing the data in a format that is suitable for the model would add a lot of overhead, such as finding the neighbors of each block or padding for boundaries. Another issue is that the block information is repeated several times in the dataset when the outputs are estimated for that block or when its neighbors are calculated. This unnecessary repeated data increases the size of the dataset and take excessive time in the preparation process.

In this scenario, a CNN-based model is proposed to address these two issues. By using convolutional layers, the entire reservoir can be processed in each step. Because of the overlap scan pattern for the convolutional operation, the time and effort used to prepare the input data for the model are reduced with no repeated data. As shown in Fig. 5, the model follows the same numbers of neurons and activation functions shown in Table 6. To follow the pattern of 8-surrounding neighbors (Fig. 4c), a 3×3 convolutional layer is used in the first four layers, while 1×1 convolutional operations are utilized in other layers. Additionally, a skip connection is utilized for faster learning. To preserve the given dimension of the reservoir, a zero-padding technique is used.

4. Experiment setup

In this work, the pressure and the saturation values of each fluid at each block in the reservoir are estimated during continuous production via the proposed NN models. The data necessary to train and test the proposed model is generated using a numerical simulator called CMG. Two types of reservoir models are studied: radial and cartesian. For the radial reservoirs, a homogeneous approach in which the parameters are kept constant for all blocks in the entire reservoir is used. For Cartesian reservoirs, both homogeneous and heterogeneous approaches are considered. The parameters of each block in a heterogeneous reservoir are randomly sampled from a uniform distribution function. These parameters are porosity, permeability *I*, permeability *J*, and permeability *k*, where *I*, *J*, and *k* are the three basic directions. The ranges of values used for the uniform distribution are shown in Table 7. The uniform distribution ensures that all values within these ranges are equally represented in the data. Therefore, their effect will be learned by the model without any biasing.

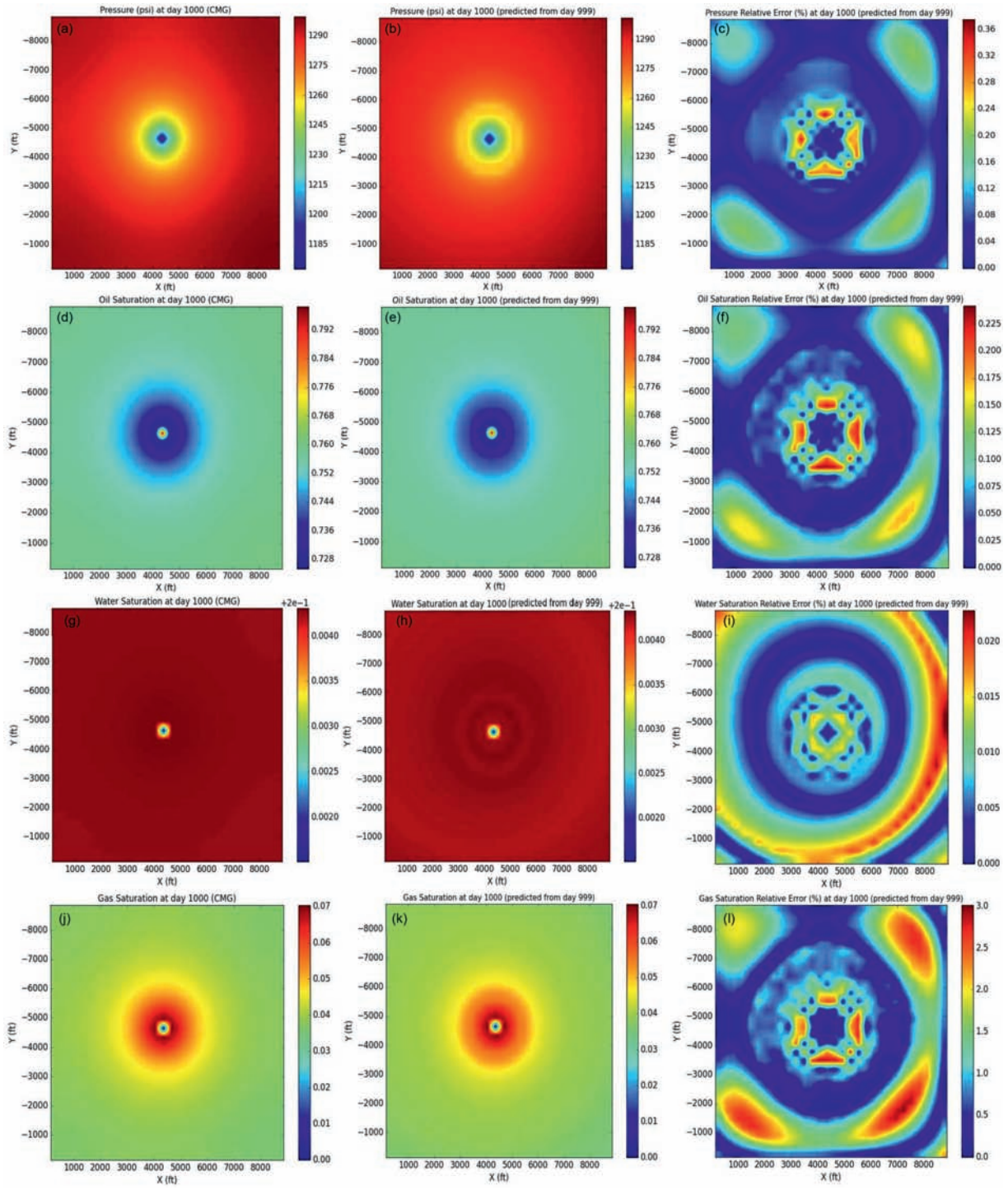


Fig. 12. One-day prediction rock and fluid properties for the third scenario.

For each scenario, CMG is used to generate a dataset of the daily pressure and fluid saturation values for 10 years. This dataset is divided into two halves to form training and testing datasets. The training dataset is used to train the previously proposed models to estimate those values of reservoir properties for a horizon of one day. In contrast, the test dataset is used to evaluate the model's performance. Although the estimation horizon of the model is just one day, it can be used in a recursive way to extend the estimation to even longer periods. The metric used to evaluate the models is the mean absolute percentage error (MAPE), which is given by equation (1).

$$MAPE = \frac{1}{n}\sum_{i=1}^{n}\frac{\left|\boldsymbol{X}_i - \widehat{\boldsymbol{X}}_i\right|}{|\boldsymbol{X}_i| + \epsilon} * 100\ \% \tag{1}$$

where $\boldsymbol{X}_i$ and $\widehat{\boldsymbol{X}}_i$ indicate the actual and predicted data, respectively, n represents the number of the input/output pairs, and ϵ is a small positive value to avoid division by zero.

Here, we present the advantages of combining CNNs and RNNs.; (1) In addition to learning local spatial dependencies within pressure and saturation fields, CNNs are very good at

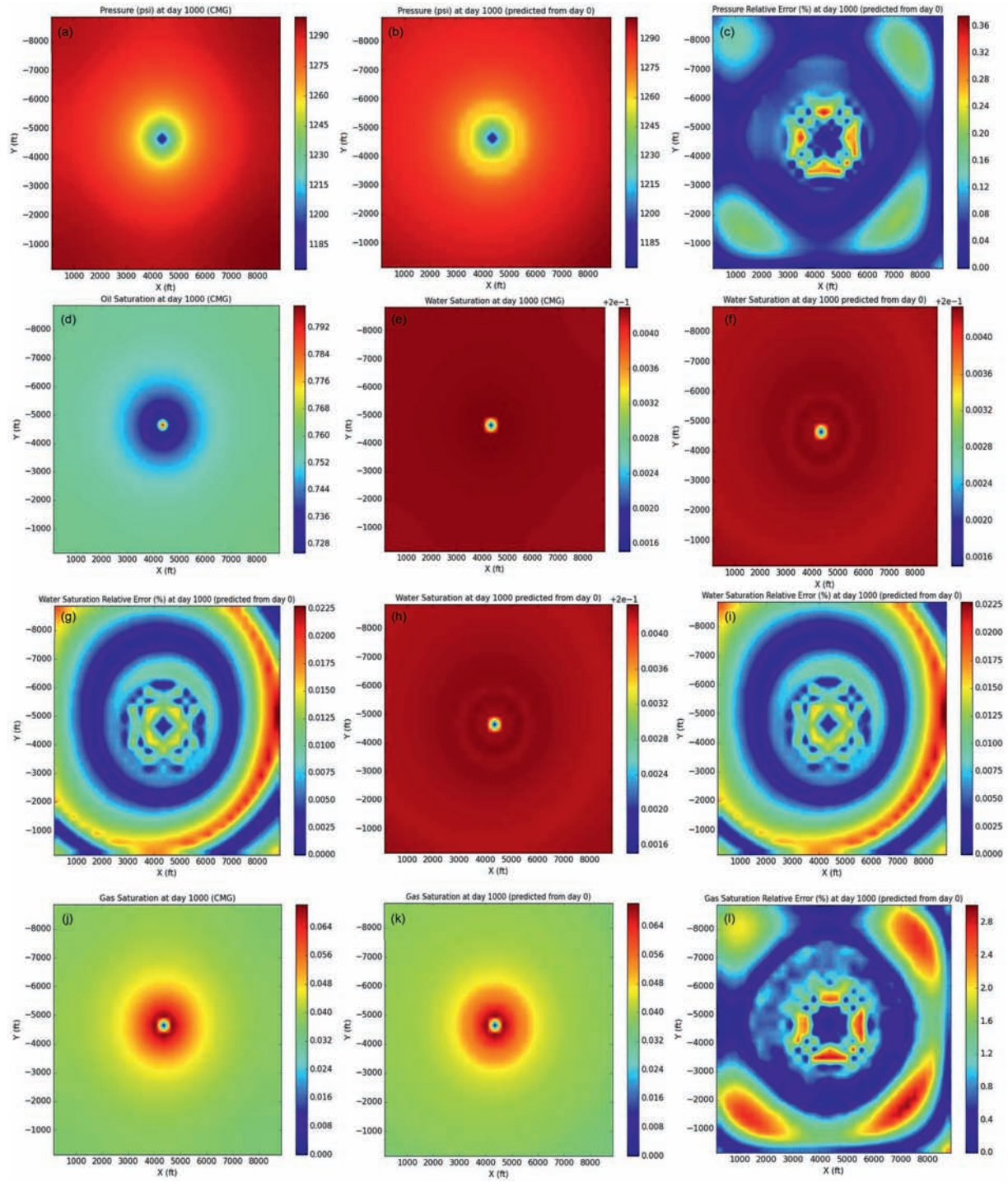


Fig. 13. 1000-day prediction rock and fluid properties for the third scenario.

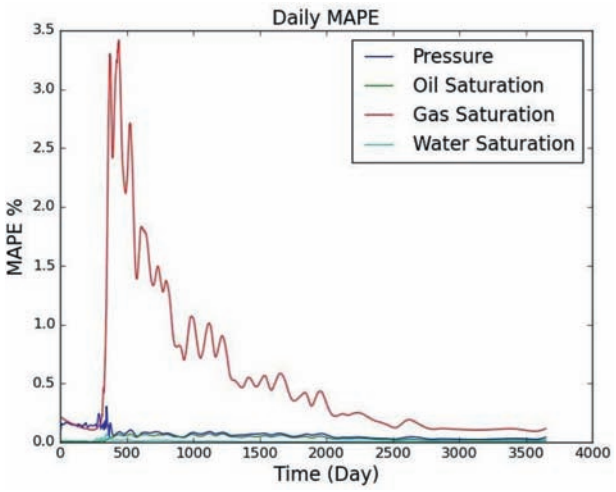


Fig. 14. The accumulated MAPE of the fluid flow third scenerio.

Table 11
Mean absolute percentage error value for each output prediction.

	Training data (50 %)	Testing data (50 %)
Pressure	0.03637 %	0.03650 %
Oil saturation	0.01866 %	0.01872 %
Water saturation	0.00970 %	0.00975 %
Gas saturation	0.44912 %	0.45114 %

capturing spatial heterogeneities in reservoir parameters (such as permeability and porosity). (2) RNNs can describe temporal dynamics by observing how these spatial properties change throughout the course of production, especially LSTMs or Gated Recurrent Units (GRUs). (3). (5) Conventional methods frequently call for recursive numerical solvers for every time step. By implicitly learning from prior time steps, CNN–RNN models can increase prediction speed and minimize computing load. (6) This architecture's scalability for long-term production simulation can be enhanced by training it to predict multiple future states at once. (7) RNNs assist in adapting to time-varying boundary conditions (such as injection rate and production restrictions), but CNNs do well in generalizing across spatial domains with comparable statistical properties. (8) The model is resilient and portable because of its combined ability to generalize across various reservoir geometries, injection techniques, and well configurations. (9) Sequential time series are commonly used to record field and simulation data. RNNs are perfect for combining with CNN-derived spatial embeddings to forecast changing flow behavior because they are built to process such sequences. (10) For reservoir diagnostics, CNN layers offer intermediate spatial representations that may be seen and analyzed. Engineers can comprehend the timing of water breakthrough, pressure decline, and sweep efficiency progression thanks to RNN outputs' ability to analyze temporal trends.

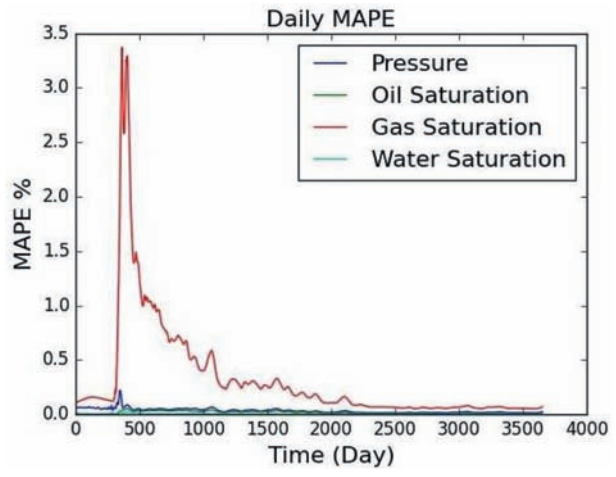


Fig. 15. The accumulated MAPE of the fluid flow fourth Scenerio.

5. Results and discussion

This section lists the results of applying the proposed model for each scenario. For each scenario, the MAPE of the estimated output for a horizon of one day is calculated for both the training and testing datasets. For a one-day prediction, Fig. 6 illustrates how the predicted values are distributed within the reservoir compared with those produced by CMG. The relative percentage error is also shown for each grid block. The same set of results is presented in Fig. 7, but in a recursive mode in which the output is estimated for a longer period (i.e., 1500 or 2000 days). In this mode, we start with the information of the first day (day 0) and use it to predict the next day, i.e., day 1. Then, we use the predicted output to predict the output of the day after (day 2) and so on until the final day is reached. Two criteria are used to determine the final date for the recursive mode: (1) the time is long enough to complete a lengthy series of subsequent forecasts, and (2) the period is short enough for the reservoir to run out. This proves that the model can be used for prediction over a longer period without losing much accuracy. Of course, the error will be more than that of a one-day prediction because of error accumulation.

5.1. Fluid flow for a homogeneous radial model ignoring relative permeability

Table 8 shows the MAPE for each estimated output calculated over the entire dataset. The training error values are less than 0.15 % for all predicted values, which reveals that the proposed model learned how the pressure and fluid are distributed within the reservoir and how they change during production. The error of the testing dataset is also less than 0.15 %, implying that the model achieves the generality goal. The first column of Fig. 6 illustrates how the pressure and fluid flow are distributed within the whole reservoir calculated using CMG versus a one-day prediction using the proposed NN model. The second column shows the relative error calculated at each reservoir's sector due to that prediction. The maximum percentage error is less than 0.25 % for all predicted values. Fig. 7 is similar to Fig. 6 but for a 2000 recursive prediction. The maximum error in this recursive prediction increased to 1.2 %.

Fig. 8 illustrates how the daily error accumulates over a period of 10 years in a recursive prediction mode given only the initial pressure and fluid saturation. The errors are less than 1 % for all values except for the initial gas saturation due to the low gas saturation, which means that even a small difference in absolute magnitude can lead to a high error percentage.

5.2. Fluid flow for a homogeneous radial model by considering relative permeability

For the second scenario, the MAPE values are less than 0.5 % for all estimated outputs for both the training and testing datasets (Table 9). This is higher than the first scenario but still in the acceptable range. This difference is due to an increase in the

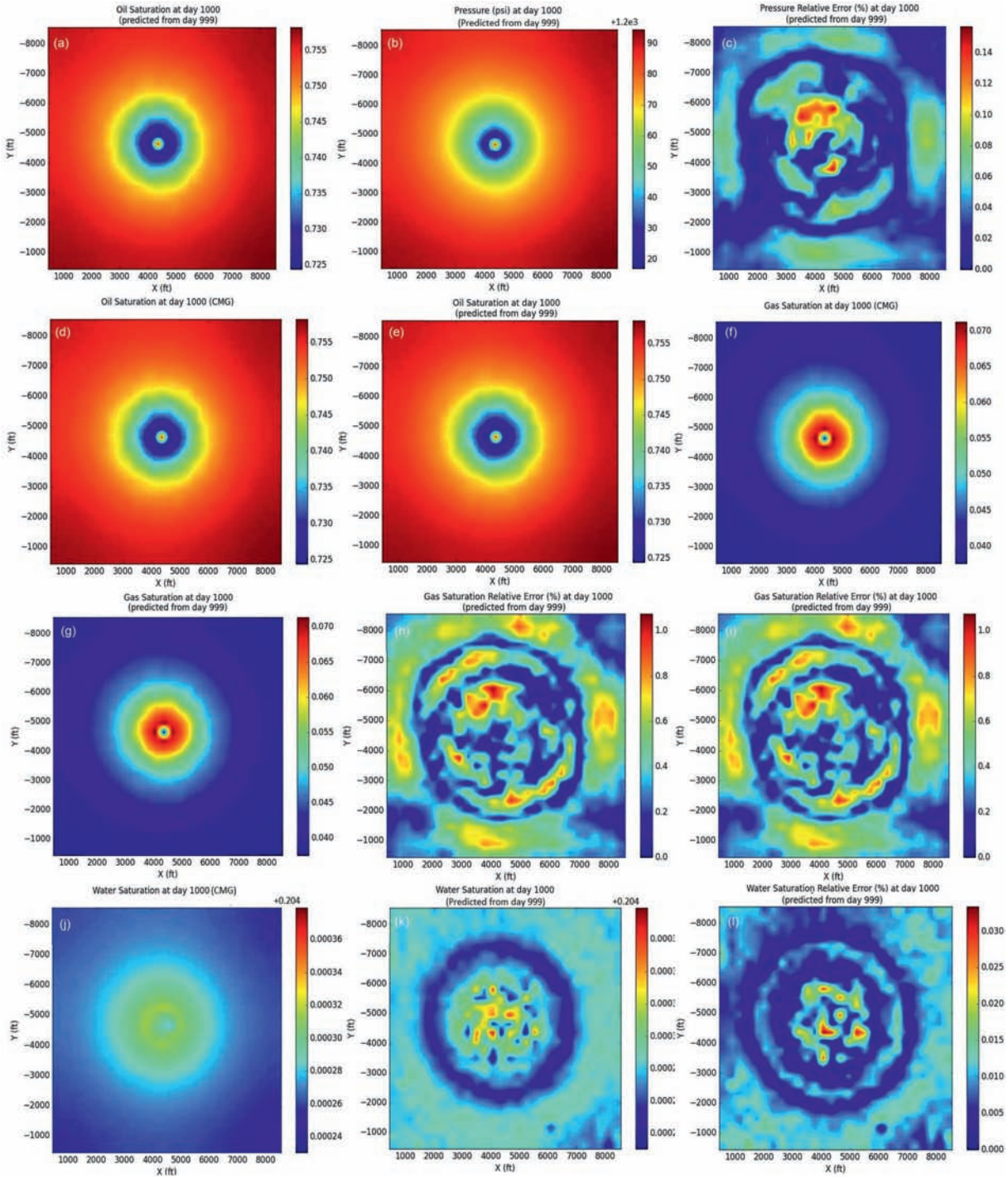


Fig. 16. One-day prediction rock and fluid properties for the fourth scenario.

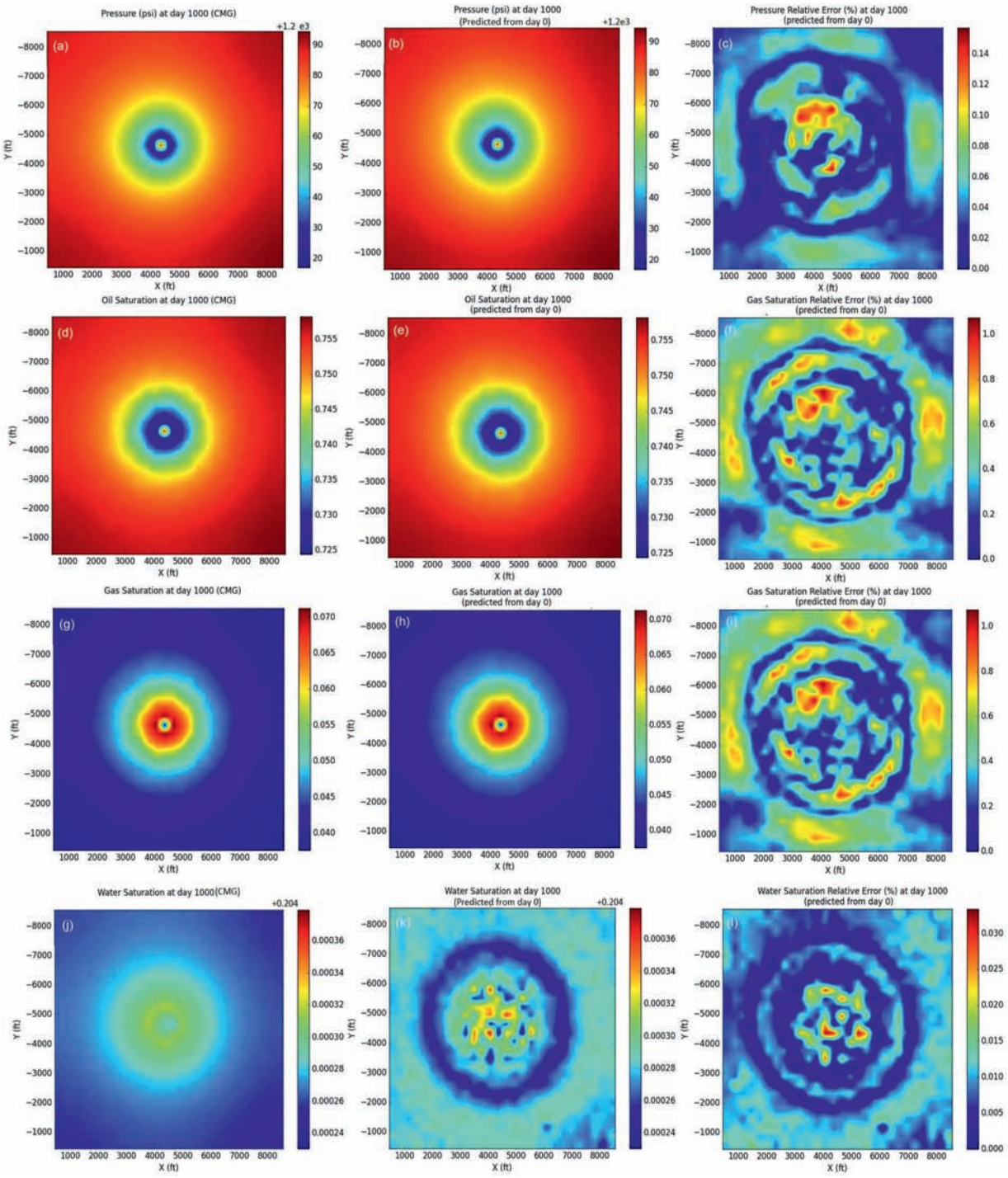


Fig. 17. 1000-day prediction rock and fluid properties for the fourth scenario.

Table 12
Mean absolute percentage error value for each output prediction.

	Training data (50%)	Testing data (50%)
Pressure	0.12647 %	0.13131 %
Oil saturation	0.02967 %	0.03066 %
Water saturation	0.06394 %	0.06708 %
Gas saturation	0.73594 %	0.87408 %

complexity of the problem. Fig. 9 shows the predicted pressure and saturation for each fluid within the reservoir using CMG versus those predicted by the model and the relative error for a one-day horizon estimation. The maximum percentage error is less than 0.5 % for all predicted values, again higher than the first scenario. Fig. 10 shows the same but for 2000 daily successive

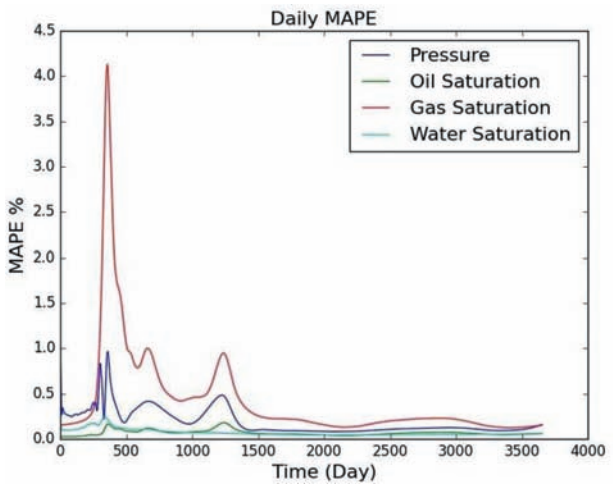


Fig. 18. The accumulated MAPE of the fluid flow for fifth scenerio.

estimations. The maximum error reaches 1.1 %.

Fig. 11 illustrates the daily MAPE error for the recursive prediction for the reservoir that evolves over 10 years of production. As in the first scenario, the maximum error value is still less than 7 %, but the average error is higher. This highest error rate is still in the prediction of gas saturation in the beginning.

5.3. Fluid flow prediction for a cartesian single-layer homogeneous reservoir using DNN

The MAPE errors evaluated for the datasets for a one-day horizon prediction are shown in Table 10. The error values evaluated over both datasets are less than 0.2 % for all predicted values, which is still acceptable. Each image in Figs. 12 and 13 shows the reservoir in which each pixel represents a grid block, and the color associated with that pixel indicates the pressure or saturation value of a certain fluid in that grid. The color bar at the right of each image maps the color to a given value. From left to right, the images in Fig. 12 are the values calculated by CMG, those predicted by the proposed model over a one-day horizon, and the relative error for each grid block. The rows from top to bottom illustrate the pressure, oil saturation, water saturation, and gas saturation. Fig. 13 follows the same pattern but for 1000 successive predictions from day 0 until day 1000. The maximum percentage error is less than 3 %.

The daily MAPE of the recursive prediction for the reservoir over 10 years is shown in Fig. 14. The maximum error value is still less than 3.5 %. Fig. 13 shows the distribution of the predicted values over the whole reservoir after a 2000-day recursive prediction compared with CMG values and the percentage error due to this recursive prediction in the same manner as in previous scenarios. The maximum error in this recursive prediction increased to 3 %.

5.4. Fluid flow prediction for a cartesian single-layer heterogeneous reservoir using DNN

The prediction error increases as the model becomes more complex for a heterogeneous reservoir, especially in the recursive mode. Table 11 shows that the MAPE for all predicted reservoir properties for a one-day horizon prediction is still small (less than 0.5 % for all the predicted values). Following the same pattern described before for Figs. 12 and 13, the pressure and fluids distributed within the reservoir for the 1000-day horizon prediction are obtained in the set of images included in Figs. 16 and 17. Fig. 16 indicates that the relative error for a one-day prediction is less than 1 % for all blocks within the reservoir for all predicted values. The same results can obtain using the recursive prediction mode after 1000 consequent predictions, as shown in Fig. 17. According to Fig. 15, the maximum daily estimation error recursively estimating the pressure and saturation of the fluids within the reservoir over 10 years has a maximum daily estimation error is less than 3.5 %.

5.5. Fluid flow prediction for a cartesian single-layer heterogeneous reservoir using CNN

Using a CNN enables us to implement a more complex model with a higher hierarchy and to utilize skip connections. It also eliminates the overhead of preparing the spatial data for the feedforward model used in the previous subsection. The prediction of the boundary blocks, which were previously neglected, is considered in this model. Table 12 shows that the MAPE for a one-day horizon prediction is less than 0.9 % for all values. Fig. 19 provides an example of a one-day forecast. In this example, the relative error is less than 4.5 % for all the reservoir blocks and all predicted values. The same example is repeated for a recursive prediction mode lasting 1000 days. The relative error for the estimated quantities is included in Fig. 20. The maximum error in this recursive prediction increased to 5.5 % but is still in the acceptable range. The daily MAPE utilizing this mode is shown in Fig. 18 for the reservoir over 10 years, with a maximum value of less than 4 %. Table 13 describes the comparison between traditional and our proposed data driven model.

5.6. Interpretation of results and implications for reservoir management

A variety of heterogeneous reservoir scenarios were successfully predicted by the suggested hybrid CNN–RNN model in terms of fluid saturation and pressure distribution over time. In addition to serving as a stand-in for computationally costly full-physics simulations, these forecasts offer insightful information about reservoir behavior that is pertinent to field development planning. The anticipated physical trends in single-layer heterogeneous reservoirs in situations of water flooding were reflected by model forecasts. For instance, both simulation and model projections showed that areas with poorer permeability saw slower water front progress and a delayed pressure reduction.

The model's capacity to implicitly learn permeability contrasts and their impact on multiphase flow was demonstrated by the temporal changes in saturation profiles that corresponded with the heterogeneity patterns. The algorithm identified areas of early water breakthrough and low sweep efficiency—two important markers of oil that have been omitted from the saturation maps over time. These understandings are essential for choosing zones for conformity control interventions, such as gel or polymer treatments, or for determining infill drilling targets. Proactive operational adjustments to improve recovery are made possible by the capacity to forecast such qualities. Decisions about fluid injection rates and well placement can be supported by the model's near-real-time forecasting results. Operators can postpone water breakthrough, maintain reservoir pressure, and optimize injection techniques by anticipating localized pressure fall or saturation buildup. This supports EOR techniques by using predictive modeling to improve the time and placement of gas or water injection.

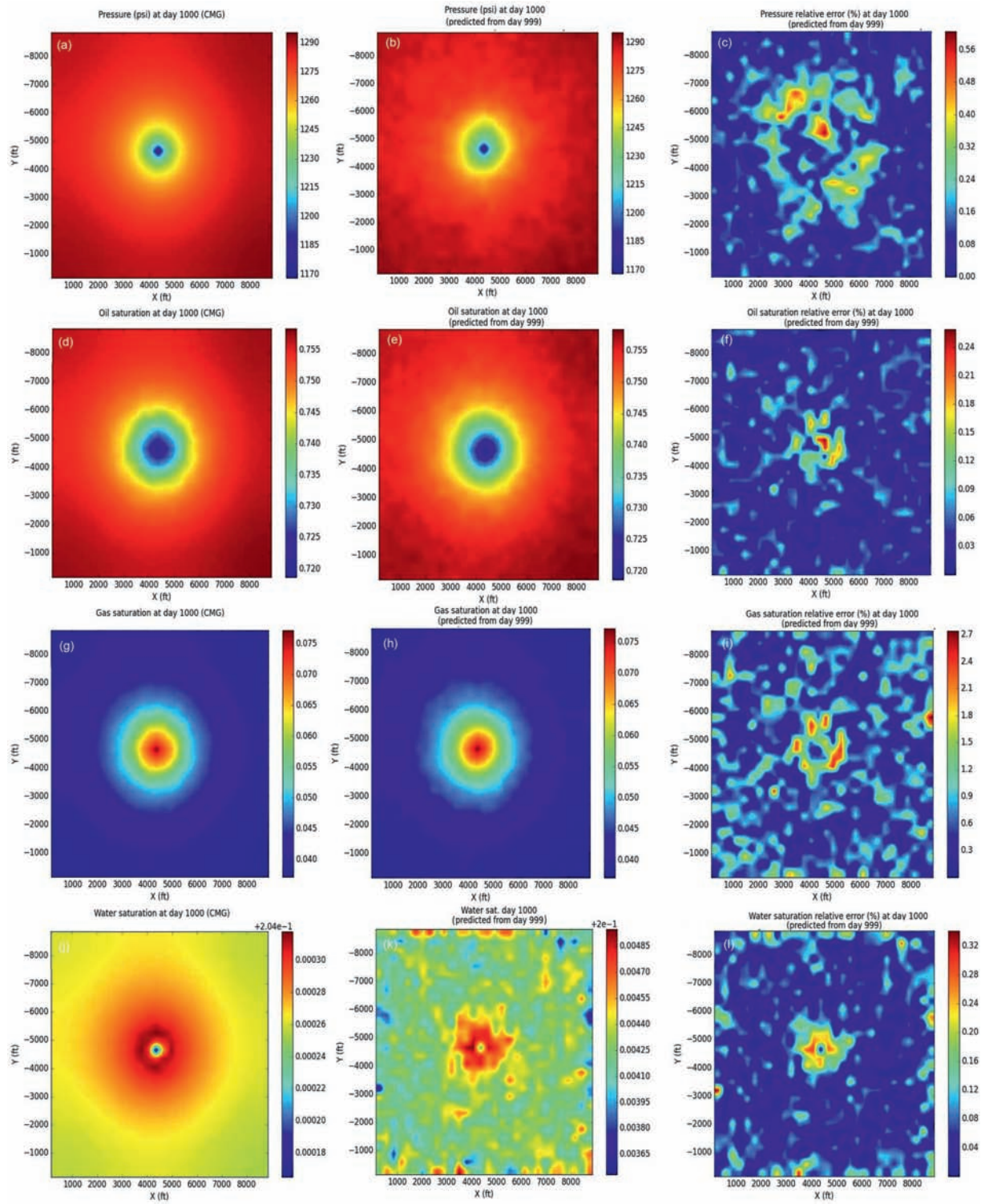


Fig. 19. One-day prediction rock and fluid properties for the fifth scenario.

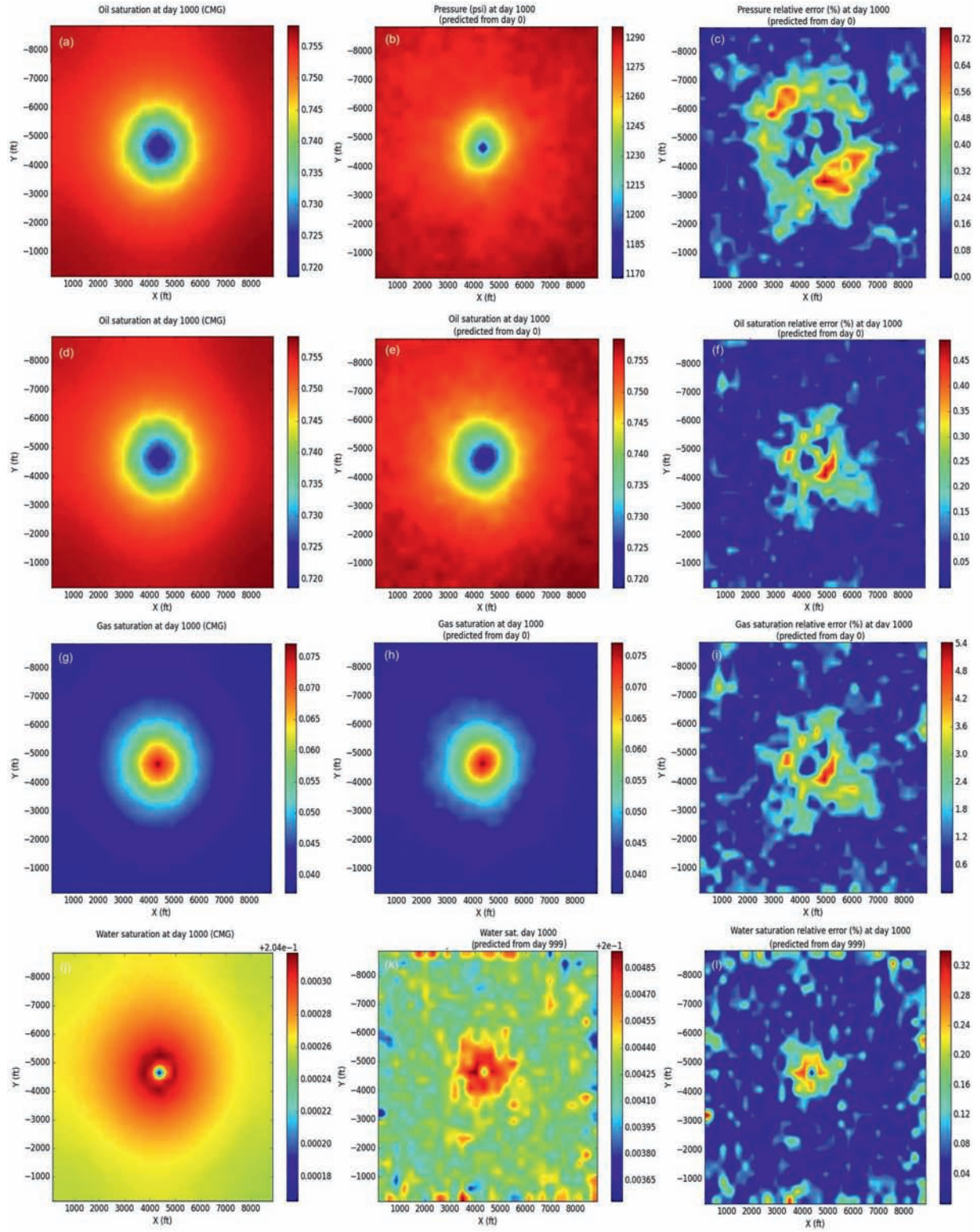


Fig. 20. 1000-day prediction rock and fluid properties for the fifth scenario.

Table 13
Comparison of Traditional Reservoir Engineering vs. Proposed Data-Driven Method.

Criteria	Traditional Reservoir Engineering	Proposed Data-Driven Method (This Study)
Production Condition Assumption	Typically assumes steady-state or pseudo-steady-state	Explicitly models unsteady-state conditions
Pressure Prediction Scope	Bulk-average reservoir pressure	Fine-scale pressure prediction at each individual grid block
Saturation Estimation	Generally simplified or average-based	Grid-level saturation distribution using time-dependent data
Modeling Resolution	Homogeneous reservoir assumptions	Captures heterogeneity in pressure and saturation at a high resolution
Applicability to Transient Conditions	Limited accuracy in dynamic (transient) states	Designed to handle transient pressure and saturation changes
Computational Speed	Fast but lacks spatial detail	Slightly higher cost but optimized for high accuracy in spatial domains
Error Tracking (Unsteady-State)	Typically lacks grid-specific error analysis	Includes daily pressure prediction with relative error at the grid level
Innovative Contribution	Relies on analytical solutions and coarse modeling assumptions	Integrates machine learning to reflect real-time dynamic behavior

6. Conclusions

In addition to numerical modeling, this work offered an additional method for quickly and reliably predicting reservoir water, oil, gas saturation, and pressure distribution. These predictions were created using a deep neural network model with feedforward and CNN layers. The dataset derived from a simulation was used for model training and testing. It was found that it is possible to anticipate reservoir properties faster using the trained model than using numerical simulation.

When predicting water, oil, and gas saturations and pressure distribution throughout the reservoir, the DNN provides a fast, general method that can be used for both heterogeneous and homogeneous reservoirs. A simple model with feedforward layers can be used with acceptable results for a simple and specific reservoir type. For a more general reservoir model, a CNN provides a better solution that offers good results and reduces the computational time needed for data preparation in each iteration.

The developed models have proven to be accurate and reliable for an extended prediction period. Based on model validation, the models can forecast water, oil, gas saturation, and pressure distribution and offer clues for where to access residual oil in future production. Thus, machine learning approaches provide significant computational time benefits over numerical simulation, as the trained models can be utilized for other reservoir settings.

CRediT authorship contribution statement

Arifur Rahman: Writing – review & editing, Writing – original draft, Visualization, Validation, Software, Methodology, Investigation, Formal analysis, Data curation, Conceptualization. **George Daoud:** Writing – review & editing, Writing – original draft, Validation, Software, Methodology, Investigation, Formal analysis, Data curation. **Ezeddin Shirif:** Writing – review & editing, Supervision, Software, Resources, Project administration, Funding acquisition, Conceptualization. **Mohamed El-Darieby:** Writing – review & editing, Supervision, Software, Resources, Project administration, Funding acquisition. **Mohamed El-Hendawi:** Software, Resources, Formal analysis.

Declaration of competing interest

We confirm that there are no conflicts of interest.

Acknowledgments

This research was funded by the nonprofit Petroleum Technology Research Center (PTRC, https://ptrc.ca/) and the nonprofit Mitacs Center for Research (https://www.mitacs.ca/).

References

Aizenberg, I., Aizenberg, N., Vandewalle, J., 2000. *Multi-Valued and Universal Binary Neurons*. Kluwer Academic Publishers. https://doi.org/10.1007/978-1-4757-3115-6.

Al-Zawawi, A.,S., Hayder, M.E., Baddourah, M.A., 2011. Using streamline and reservoir simulation to improve waterflood management. In: SPE Middle East Oil and Gas Show and Conference. https://doi.org/10.2118/141794-ms.

Almulhim, A., Alharthy, N., Tutuncu, A.N., Kazemi, H., 2014. Impact of imbibition mechanism on flowback behavior: a numerical study. In: SPE-30th Abu Dhabi International Petroleum Exhibition and Conference, ADIPEC 2014: Challenges and Opportunities for the next 30 Years. https://doi.org/10.2118/171799-ms.

Archie, G.E., 1947. Electrical resistivity an aid in core-analysis interpretation. AAPG (Am. Assoc. Pet. Geol.) Bull. 31 (2), 350–366. https://doi.org/10.1306/3d93395c-16b1-11d7-8645000102c1865d.

Baldwin, J.L., Otte, D.,N., Wheatley, C.L., 1989. Computer Emulation of Human Mental Processes. Application of Neural Network Simulators to Problems in Well Log Interpretation. Society of Petroleum Engineers of AIME. https://doi.org/10.2523/19619-ms.

Chen, Z., Huan, G., Ma, Y., 2006. Computational Methods for Multiphase Flows in Porous Media. Computational Methods for Multiphase Flows in Porous Media. Society for Industrial and Applied Mathematics. https://doi.org/10.1137/1.9780898718942.

Ciregan, D., Meier, U., Schmidhuber, J., 2012. Multi-column deep neural networks for image classification. In: Proceedings of the IEEE Computer Society Conference on Computer Vision and Pattern Recognition. https://doi.org/10.1109/CVPR.2012.6248110.

Du, S., Lee, J., Li, H., Wang, L., Zhai, X., 2019. Gradient descent finds global minima of deep neural networks. In: 36th International Conference on Machine Learning, ICML, 2019.

Edwards, D.A., Gunasekera, D., Morris, J., Shaw, G., Shaw, K., Walsh, D., Fjerstad, P. A., Kikani, J., Franco, J., Hoang, V., Quettier, L., 2011. Reservoir simulation: keeping pace with oilfield complexity. Oilfield Rev. 23 (4), 4–15.

Ertekin, T., Abou-Kassem, J., King, G., 2001. Basic Applied Reservoir Simulation. Society of Petroleum Engineers.

Gharbi, R.B., Elsharkawy, A.M., 1997. Neural-network model for estimating the PVT properties of Middle East crude oils. SPE Reservoir Eval. Eng. 1 (3), 151–166. https://doi.org/10.2523/37695-ms.

Glushkov, D.O., Kosintsev, A.G., Kuznetsov, G.V., Vysokomorny, V.S., 2021. Experimental research and numerical simulation of gel fuel ignition by a hot particle. Fuel 291. https://doi.org/10.1016/j.fuel.2021.120172.

Heseldin, G.M., 1974. Method of averaging capillary pressure curves. Log. Anal. 15 (4).

Karimi-Fard, M., Durlofsky, L.J., Aziz, K., 2004. An efficient discrete-fracture model applicable for general-purpose reservoir simulators. SPE J. 9 (2). https://doi.org/10.2118/88812-PA.

Leverett, M.C., 1941. Capillary behavior in porous solids. Trans. AIME 142 (1). https://doi.org/10.2118/941152-g.

Lim, J.S., Kim, K., 2004. Reservoir porosity and permeability estimation from well logs using fuzzy logic and neural networks. In: SPE Asia Pacific Oil and Gas Conference and Exhibition. https://doi.org/10.2523/88476-ms.

Liu, H., Wu, S., 2015. The numerical simulation for multi-stage fractured horizontal well in low permeability reservoirs based on modified Darcy's equation. In: Society of Petroleum Engineers - SPE/IATMI Asia Pacific Oil and Gas Conference and Exhibition. https://doi.org/10.2118/176269-ms.

Liu, Y., Leung, J., Chalaturnyk, R., Virues, C., 2017. Fracturing fluid distribution in shale gas reservoirs due to fracture closure, proppant distribution and gravity segregation. In: SPE Unconventional Resources Conference. https://doi.org/10.2118/185043-ms.

Mohaghegh, S.D., Goddard, C., Popa, A., Ameri, S., Bhuiyan, M., 2000. Reservoir characterization through synthetic logs. SPE J. https://doi.org/10.2118/65675-MS.

Nagi, J., Kiong, T.S., Ahmed, S.K., Nagi, F., 2009. Prediction of PVT properties in crude oil systems using support vector machines. In: ICEE 2009 - Proceeding

2009 3rd International Conference on Energy and Environment: Advancement Towards Global Sustainability. https://doi.org/10.1109/ICEENVIRON.2009.5398681.
Nikravesh, M., Kovscek, A.R., Johnston, R.M., Patzek, T.W., 1996. Prediction of formation damage during fluid injection into fractured, low permeability reservoirs via neural networks. In: SPE Formation Damage Control Symposium. Lafayette, Louisiana. https://doi.org/10.2118/31103-ms.
Omurlu, C., Baran, J., Nguyen, Q., 2012. Adsorption of surface functionalized silica nanoparticles onto mineral surfaces and decane/water interface. J. Nanoparticle Res. 14 (11). https://doi.org/10.1007/s11051-012-1246-1.
Patoary, M.N.I., Tropper, C., Lin, Z., McDougal, R., Lytton, W., 2015. Neuron time warp. In: Proceedings of the Winter Simulation Conference. https://doi.org/10.1109/WSC.2014.7020177.
Rahman, A., 2012. Pressure derivative analysis with type curves for reservoir parameters estimation of Kailastila gas field, 2 (7), 139–143.
Rahman, A., Happy, F.A., Ahmed, S., Hossain, M.E., 2017. Development of scaling criteria for enhanced oil recovery: a review. J. Petrol. Sci. Eng. 158, 66–79. https://doi.org/10.1016/j.petrol.2017.08.040.
Rahman, A., Happy, F.A., Hira, M.A., Hossain, M.E., 2017. An investigation of pressure and production data using decline and type curve analysis. In: Proceedings of the International Conference on Offshore Mechanics and Arctic Engineering. https://doi.org/10.1115/OMAE2017-62472.
Rahman, A., Ahmed, S., Hossain, M.E., Happy, F.A., 2020. Development of scaling criteria for steam flooding EOR process. J. Pet. Explor. Prod. Technol. 10 (8). https://doi.org/10.1007/s13202-020-00909-1.
Riviere, B., 2007. Book review: computational methods for multiphase flows in porous media. Math. Comput. 76. https://doi.org/10.1090/s0025-5718-07-02042-x.
Roth, G., Tarantola, A., 1992. Inversion of seismic waveforms using neural networks. In: 1992 SEG Annual Meeting. https://doi.org/10.1190/1.1822218.
Sadiq, T., Nashawi, I.S., 2007. Using neural networks for prediction of formation fracture gradient. In: SPE/CIM International Conference on Horizontal Well Technology. https://doi.org/10.2523/65463-ms. Calgary, Alberta, Canada.
Samuel, A.L., 2000. Some studies in machine learning using the game of checkers. IBM J. Res. Dev. 44 (1–2). https://doi.org/10.1147/rd.441.0206.
Smith, L., Topin, N., 2016. Deep convolutional neural network design patterns. In: ICLR2017. http://arxiv.org/abs/1611.00847.
Sultan, M.A., Al-Kaabi, A.U., 2002. Application of neural network to the determination of well-test interpretation model for horizontal Wells. In: SPE Asia Pacific Oil and Gas Conference. https://doi.org/10.2523/77878-ms.
Tian, Z.Q.K., Zhou, D., 2021. Library-Based Fast Algorithm for Simulating the Hodgkin-Huxley Neuronal Networks. http://arxiv.org/abs/2101.07257.
Tu, Z., Xie, W., Zhang, D., Poppe, R., Veltkamp, R.C., Li, B.X., Yuan, J.S., 2019. A survey of variational and CNN-based optical flow techniques. Signal Process. Image Commun. 72. https://doi.org/10.1016/j.image.2018.12.002.
Tuero, F., Crotti, M.M., Labayen, I., 2017. Water imbibition EOR proposal for shale oil scenarios. In: SPE Latin American and Caribbean Petroleum Engineering Conference Proceedings. https://doi.org/10.2118/185560-ms.
Yuan, C., Delshad, M., Wheeler, M.F., 2010. Parallel simulations of commercial-scale polymer floods. In: Society of Petroleum Engineers Western North American Regional Meeting 2010 - in Collaboration with the Joint Meetings of the Pacific Section AAPG and Cordilleran Section GSA. https://doi.org/10.2523/132441-ms.
Zhang, D., 2019. Fundamentals of Image Data Mining. Springer, Cham. http://link.springer.com/10.1007/978-3-030-17989-2.
Zhang, F., Saputra, I.W.R., Niu, G., Adel, I.A., Xu, L., Schechter, D.S., 2018. Upscaling laboratory result of surfactant-assisted spontaneous imbibition to the field scale through scaling group analysis, numerical simulation, and discrete fracture network model. In: Proceedings of SPE Symposium on Improved Oil Recovery. https://doi.org/10.2118/190155-ms.
Zhou, C.D., Wu, S.L., Zhang, C.M., Zhu, D.H., Zhang, Y.X., 1994. Direct identification of hydrocarbon from well logs: a neural network interpretation approach. In: Annual Technical Meeting 1994. https://doi.org/10.2118/94-53.